Structure and Dynamics of Water/Methanol Mixtures at Hydroxylated Silica Interfaces Relevant to Chromatography

Prashant Kumar Gupta[†,‡] and Markus Meuwly[*,†]

Department of Chemistry, University of Basel, Klingelbergstrasse 80, CH-4056 Basel, Switzerland

E-mail: m.meuwly@unibas.ch

Abstract

The spectroscopy and dynamics of water/methanol (MeOH) mixtures at hydroxylated silica surfaces is investigated from atomistic simulations. The particular focus is on how the structural dynamics of MeOH changes when comparing surface-bound and MeOH in the bulk. From analyzing the frequency frequency correlation functions it is found that the dynamics on the picosecond time scale differs by almost a factor of two. While the relaxation time is 2.0 ps for MeOH in the bulk solvent it is considerably slowed-down to 3.5 ps for surface-bound MeOH. Surface-adsorbed MeOH molecules reside there for several nanoseconds and their H-bonds are strongly oriented towards the surface-OH groups. These results are of particular relevance for chromatographic systems where the solvent may play a central role in their function. The present simulations suggest that surface-sensitive spectroscopic techniques should be useful in better

[*]To whom correspondence should be addressed

[†]Department of Chemistry, University of Basel, Klingelbergstrasse 80, CH-4056 Basel, Switzerland

[‡]Current address: Lehrstuhl für Theoretische Chemie, Ruhr-Universität Bochum, Universitätsstraße 150, D-44801 Bochum, Germany

characterizing such heterogeneous systems and provide detailed insight into solvent dynamics and structure relevant in chromatographic applications.

Introduction

The dynamics of pure and mixed solvents at the solid/liquid interface is of primary importance for fundamental and applied physico-chemical problems, including surface science (adsorption/desorption), material science, interfacial chemistry, or high performance liquid chromatography (HPLC).[1–6] It has been shown in the past that such systems are highly dynamical and exhibit properties which differ from bulk solution.[3,7,8] Specific questions concern the structure, orientation and dynamics of solvents at the solid/liquid interface, the orientational probability of the molecules (water/methanol), their residence times at the surface and the modification of their spectral signatures.[8–10] Also, it is of interest to determine the spatial organization and extent of the interfacial region and to better characterize the transition between the solid surface, the adsorbed solvent layer(s) and the bulk solvent.

For the particular situation in HPLC, the degree and chemical nature of the solvated surface has potentially important implications for selectivity. It has been suggested more than 30 years ago that solvent molecules - specifically water - can hydrate the stationary phase in realistic chromatographic columns.[11] However, direct experimental proof for this proposal is still lacking and the present work discusses one viable way to address this question quantitatively. Previous work has included thermogravimetry and infrared spectroscopy.[11] However these methods are indirect concerning the characterization of the surface layer. More recently, nonlinear spectroscopies have been used to characterize acetonitrile(ACN)/methanol(MeOH) mixtures at silica surfaces.[8] From the spectroscopic signatures of mixtures with varying mole fractions it was inferred that depending on the relative amounts of ACN and MeOH their ordering at the surface differs.

The interface between a hydroxylated silica surface and bulk solvent has attracted appreciable attention in the past both, experimentally and in simulation studies.[8,12–16] The studies included hydroxylated silica surfaces in contact with acetonitrile,[9] alcohols[12] and water[13,15,16]

and the investigation of nanoconfinement on water dynamics in hydroxylated silica pores.[14] Whenever investigated, the studies found pronounced slowdown of the dynamics of the solute near the surface.[9,14] Of particular fundamental interest is the study of water dynamics depending on the polarity and topography of the surface which was found to tune the hydrophobic/hydrophilic character of the surface.[15] Vibrational sum frequency experiments of MeOH and EtOH (ethanol) close to hydroxylated silica surfaces were able to differentiate between the two molecules at the solid/liquid interface. The absence of a spectroscopic response in the VSF spectrum for MeOH close to the SiOH surface at the solid/liquid interface was related to surface defects in the second solvent layer.[12] Finally, for water in hydrophilic and hydrophobic silica pores pronounced changes in the water reorientation dynamics was found. In particular, different from the situation in bulk, the reorientational dynamics of water in such environments exhibits multiple exponential (hydrophobic) or even nonexponential decay.[14]

A microscopic understanding of the solid/liquid interface provides insight into adsorption which plays an important role in chromatographic techniques. Molecular dynamics simulations proved to be useful to obtain molecular-level insight for such processes at an atomistic scale.[2–4,17] Different binary liquid mixtures (water/methanol or water/acetonitrile) with different mole fractions show distinct behavior for adsorption of analyte molecules by influencing their retention times.[18] This lead to the notion that understanding the role of the co-solvent in chromatographic systems is key for characterizing the separation process. Together with the surface functionalization, the concentration of co-solvent modulates the hydrophobic character and hence affects the elution of analyte molecules. Beyond the structural organization of the solvent mixtures at and near the stationary phase, continuous exchange between the bulk and the stationary phase on the pico- and nanosecond time scale has been found.[17] This leads to local heterogeneity on the microscopic scale.[19] These exchanges are due to competitive intermolecular interactions between the solvent molecules and the polar -OH

groups at the surface. As a first step towards characterizing the solvent layer close to the stationary phase in a HPLC system the idealized situation of a water/methanol mixture at a hydroxylated silica layer is investigated.

Computational Methods

The simulation system consisted of two 8.75 Å thick segments of the (101) face of a quartz crystalline lattice with dimensions of 36×41 Å and a suitable solvent mixture between them. This resulted in two surfaces with 64 silica hydroxy groups on each surface. The distance between the two silica layers was 20 Å. This arrangement was superimposed by an equilibrated water/methanol(MeOH) box containing 150 and 328 H_2O and MeOH molecules, respectively, corresponding to a mole fraction of $\approx 0.3/0.7$ and all solvent molecules overlapping with the silica layers were removed, see Figure 1. The force field for the silica system is that of a previous study.[20] For water the transferable intermolecular potential three-point (TIP3P)[21] was used and for methanol the point charges are those from the CHARMM force field.[22] As the vibrational spectroscopy of the MeOH -OH bond is of primary interest it is treated with a more realistic Morse potential $V(r) = D_e(1 - \exp[-\beta(r - r_0)])^2$ where D_e is the well dept, β characterizes the repulsive wall, and r_0 is the equilibrium bond length. For the O-H bond the following values were used $D_e = 109.4$[23] kcal/mol, $\beta = 2.254$ Å^{-1} and $r_0 = 0.97$ Å, which reproduce the experimentally known stretching frequency of 3681 cm^{-1}.[24]

All MD simulations were carried out with the CHARMM program,[25] with periodic boundary conditions (PBC) and nonbonded interactions (electrostatic and Lennard-Jones) were truncated at a distance of 10 Å and switched between 8 and 10 Å. The atomic positions of the silica layers were held fixed during the simulations except for hydrogen atoms of the silanol group. The time step for propagating Newton's equations of motion was $\Delta t = 0.5$

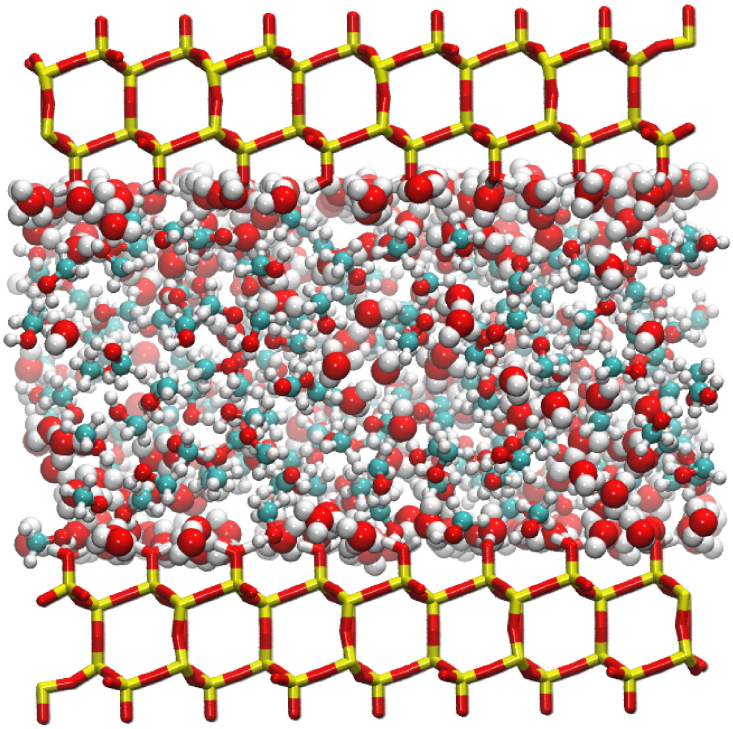

Figure 1: The bare hydroxylated silica layer with water/methanol mixture. Water molecules are in VdW, methanol in CPK, and the silica layer in licorice representation. The $z-$axis is normal to the silica surface.

fs. The system was heated for 50 ps from 0 to 300 K and equilibrated at 300 K for 500 ps. Production runs were performed for 2.5 ns in the NVT ensemble. SHAKE[26] was used to constrain all bonds involving hydrogen atoms in water and the silica layer.

For computing the spectra the frequency trajectory $\omega(t)$ was obtained from the normal modes of each snapshot included in the analysis as described before.[27] For each of the 5×10^5 snapshots along the 2.5 ns trajectory, the structure of four MeOH molecules permanently close to the silica surface (see below) is minimized while the environment is frozen in its instantaneous configuration. For every frame of the trajectory the normal modes of the selected MeOH were determined using the full interaction in the system. From this the frequency of the OH-stretching mode was determined which yields the frequency trajectory $\omega(t)$ for one particular MeOH molecule.

Results and discussion

For validation of the methods employed, the radial distribution functions (RDFs) for several atom-atom distances in bulk liquid MeOH were determined and compared with neutron diffraction experiments,[28] see Figure 2. The computational model quantitatively reproduces the experimentally determined peak positions of all RDFs. The magnitude of the first peak for the O-O and C-C RDFs underestimate those from experiments which, however, is known from previous force field-based or ab initio MD simulations.[29–31] Conversely, the height of the first oxygen-hydrogen peak is overestimated while that for the C-O RDF agrees well. However, it should also be mentioned that inversion of the experimentally determined scattering data into real space can lead to artifacts in the peak heights which will affect the comparison in Figure 2.[32]

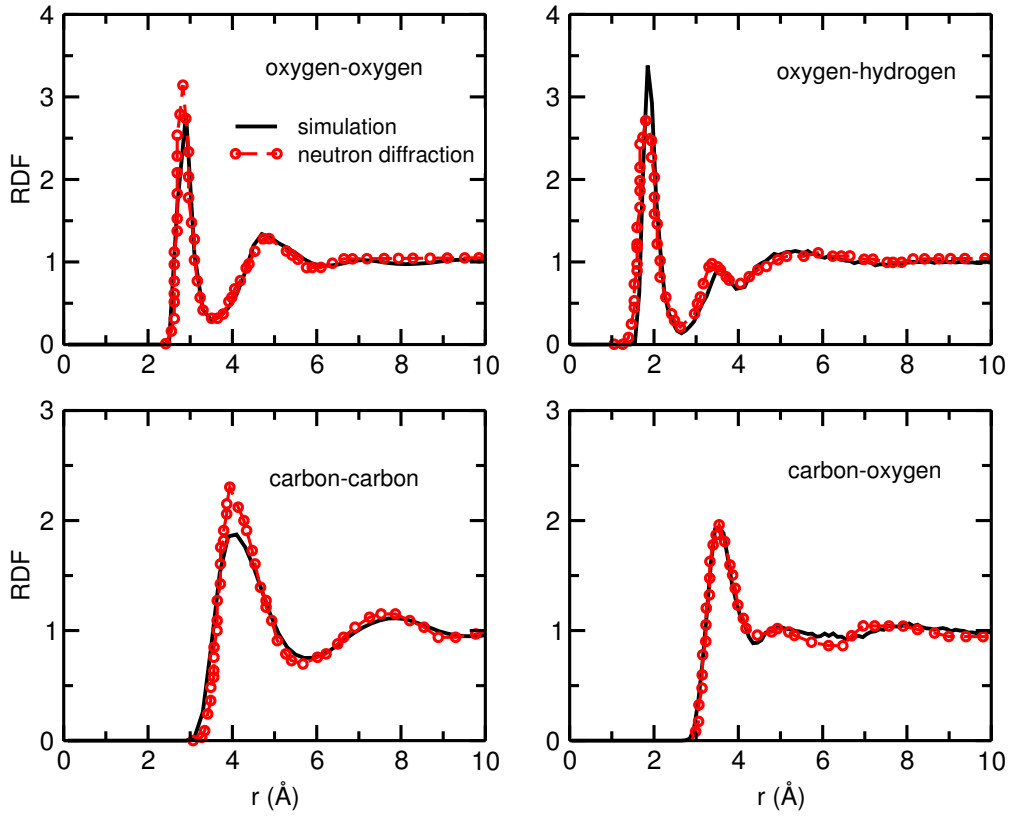

Figure 2: Different atom-atom RDFs from neutron diffraction experiments (red)[28] and from the present simulations (black).

Next, the line shape and peak positions of the 1-dimensional infrared spectra of MeOH in the gas- and liquid phase were determined, see Figure 3. Experimentally, the OH-frequency in the gas phase[33] is at 3681 $cm^{-1,}$ which shifts to 3337 cm^{-1} in pure liquid.[34] The 1-dimensional spectrum was computed from the lineshape $g(t)$

$$g\left(t\right)=\int_{0}^{t}\int_{0}^{\tau^{\prime}}d\tau^{\prime}d\tau^{\prime\prime}C(\tau^{\prime\prime}) \tag{1}$$

where $C(t)$ is the frequency frequency correlation function (FFCF) determined from the frequency trajectory $\omega(t)$

$$\begin{aligned} C\left(t\right) &= \left\langle \delta\omega\left(t_{0}\right)\delta\omega\left(t_{0}+t\right)\right\rangle_{t_{0}} \\ &= \left\langle \left(\omega\left(t_{0}\right)-\overline{\omega}\right)\left(\omega\left(t_{0}+t\right)-\overline{\omega}\right)\right\rangle_{t_{0}}. \end{aligned} \tag{2}$$

where t_0 is an arbitrary time origin, and $\delta\omega(t)=\omega(t)-<\omega>$ is the variation of $\omega(t)$ around its ensemble average $<\omega>$. The 1-dimensional infrared spectrum is then $R^{(1)}(t)\propto e^{-g(t)}$. The short lifetime[35] of the vibrationally excited state $T_1 = 0.45$ ps contributes significantly to the lineshapes. This is taken into account phenomenologically by multiplication of the linear response function with $\exp\left(-\frac{t}{2T_1}\right)$ and yields a center frequency at 3680.4 cm^{-1}, see Figure 3a (green). The effect of the condensed phase environment on the -OH peak position was determined from a pure liquid MeOH simulation in a cubic box with length 28 Å, at $T = 300$ K in the NPT ensemble. The -OH lineshape computed by averaging over 4 MeOH molecules from the pure liquid simulation is shown in Figure 3a (orange), which has a FWHM of 104 cm^{-1} and is centered around 3454 cm^{-1}, compared with a width of ~ 250 cm^{-1} and a frequency of 3337 cm^{-1} from experiment.[34] Hence, the computations qualitatively reproduce the red shift and line broadening. However, due to the approximations made in computing these spectra (cumulant and Condon (transition dipole independent of frequency) approximations), quantitative agreement can not be expected. In previous work on solvated CN^- it was found that without the cumulant approximation the linewidths typically increase by 10

% which would still not yield a considerably improved linewidth.[36] Further improvements of the force field would include a parametrization for the OH-stretch which accounts for MeOH in solution (as opposed to the parametrization for gas phase MeOH) and the use of fluctuating multipolar interactions,[37] and explicitly including polarization.[38]

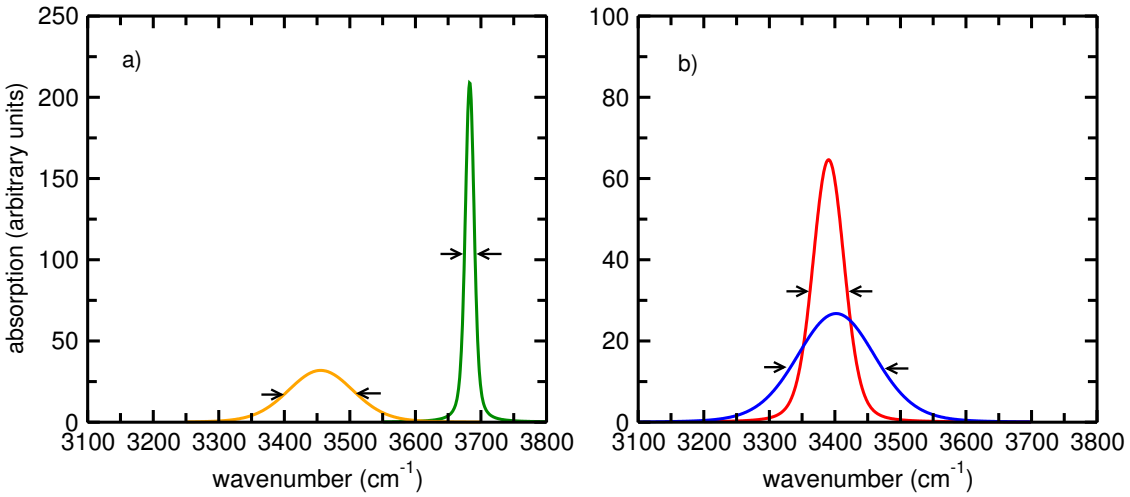

Figure 3: Panel a: Lineshape of the linear spectrum for a single MeOH in the gas phase (green, FWHM = 48 cm^{-1}, 3680.4 cm^{-1}) and average over 4 MeOH molecules in the pure MeOH liquid (orange, FWHM = 104 cm^{-1}, 3454 cm^{-1}). Panel b: lineshape of the linear spectrum averaged over 4 MeOH molecules at the hydroxylated silica interface (red, FWHM = 58 cm^{-1}, 3392 cm^{-1}) and in the binary mixture (blue, FWHM = 148 cm^{-1}, 3402 cm^{-1}). Full width at half-maximum (FWHM) and center frequencies are indicated for each lineshape.

The 1-d spectrum of liquid MeOH was previously investigated from pure MD simulations[39] and approaches combining MD and electronic structure calculations.[40] Simulations with an empirical force field yielded a red shift of 31 cm^{-1} and no FWHM was reported.[39] The simulations based on a combination of MD simulations, information from quantum chemical calculations and employing an empirical mapping between the electric field and the frequency of the -OH oscillator report the peak position at 3350 cm^{-1}, shifted by 5 cm^{-1} from the experiment and a FWHM of 226 cm^{-1}, 24 cm^{-1} smaller than the experimental value.[40] Mixed QM/MM simulations at the HF/6-31G(d) level in TIP5P water found a blue shift of 120 cm^{-1}.[41] Finally, density functional theory/MD simulations with either 32 fully deuterated MeOD molecules treated quantum mechanically or 1 MeOD surrounded by 1366

MM MeOD molecules lead to a red shift of 259 cm^{-1} and 106 cm^{-1}, respectively, compared with the experimental value of 214 cm^{-1}.[42] Depending on the functional used, DFT/MD simulations found the maximum absorption of the (broad) OD-stretch between 2500 and 2600 cm^{-1} compared to 2491 cm^{-1} from experiment which corresponds to a difference between a few and 110 cm^{-1}.[43,44] The widths of the spectra were not explicitly determined in the simulations.

The -OH lineshapes computed for MeOH at the hydroxylated silica surface and in the water-MeOH mixture are reported in Figure 3b. The FWHM of the computed spectrum is 58 cm^{-1} for surface-bound MeOH, considerably narrower than the 148 cm^{-1} for MeOH in the water-MeOH mixture. The two bands are more redshifted from gas-phase MeOH than in the pure MeOH liquid, namely by 289 and 279 cm^{-1}, respectively, compared to the peak position in the gas phase. Hence, MeOH molecules respond differently depending on the environment (pure MeOH liquid, mixed MeOH/water or MeOH close to the surface) which suggests that further optimization would allow one to bring the frequency shift into agreement with the experimentally measured red shift. However, such a fit is not the primary objective here.

For the 2D-IR spectra the response functions $R_1(t_3, t_2, t_1)$ to $R_8(t_3, t_2, t_1)$ are determined from the FFCF and a cumulant expansion truncated at second order. Only $R_1(t_3, t_2, t_1)$ to $R_6(t_3, t_2, t_1)$ correspond to the 2D IR experiment.[45,46] The response functions depend on the lineshape function $g(t)$, the frequency trajectory $\omega(t)$ and the anharmonic shift $\Delta = \nu_{01} - \nu_{12}$ and can be determined directly from sufficiently long MD simulations. For MeOH the anharmonic shift is $\Delta = 75$ cm^{-1},[47] and $g(t)$ is the lineshape function obtained from the double integration of the FFCF, see Eq. 1.

The finite lifetime of the vibrationally excited state T_1 affects the lineshape of the 2D IR signal. This is taken into account phenomenologically by multiplication of the response

functions R_i by appropriate factors which for R_1, R_2, R_4, and R_5 are

$$\exp\left(-\frac{t_1+2t_2+t_3}{2T_1}\right) \tag{3}$$

and

$$\exp\left(-\frac{t_1+2t_2+3t_3}{2T_1}\right) \tag{4}$$

for R_3 and R_6. From the response functions $R_{1,..,6}$ the associated 2D IR frequency-domain spectrum is calculated via a double Fourier transform over t_1 and t_3:[45]

$$S(\omega_3, t_2, \omega_1) = \int_0^\infty \int_0^\infty \sum_n R_n(t_3, t_2, t_1) e^{\imath\omega_1 t_1} e^{\imath\omega_3 t_3}\, dt_1\, dt_3. \tag{5}$$

The purely absorptive 2D IR spectrum

$$R_{\mathrm{abs}}(\omega_1, \omega_3) = \Re\left(R_{\mathrm{r}}(-\omega_1, \omega_3) + R_{\mathrm{nr}}(\omega_1, \omega_3)\right) \tag{6}$$

is the real part of the sum of the rephasing, R_{r}, and non-rephasing signal, R_{nr}. Using this method, spectra were obtained for waiting times t_2 ranging from 0 to 100 ps. The simulated spectra together with the center line slopes (CLS) are reported in Figure 4.

In order to characterize the environmental dynamics, the FFCF was analyzed further. Three different types of MeOH molecules were considered. Those permanently interacting with the silica surface ("surface-bound"), those always residing within the bulk ("bulk") and those changing between these two environments ("exchanging"). The averaged FFCF was fitted to a parametrized form with three time scales

$$C(t) = a_1 e^{-t/\tau_1} + a_2 e^{-t/\tau_2} + a_3 e^{-t/\tau_3} \tag{7}$$

The decay constants for surface-bound MeOH are $\tau_1 = 0.15$, $\tau_2 = 3.48$ and $\tau_3 = 42.45$ ps

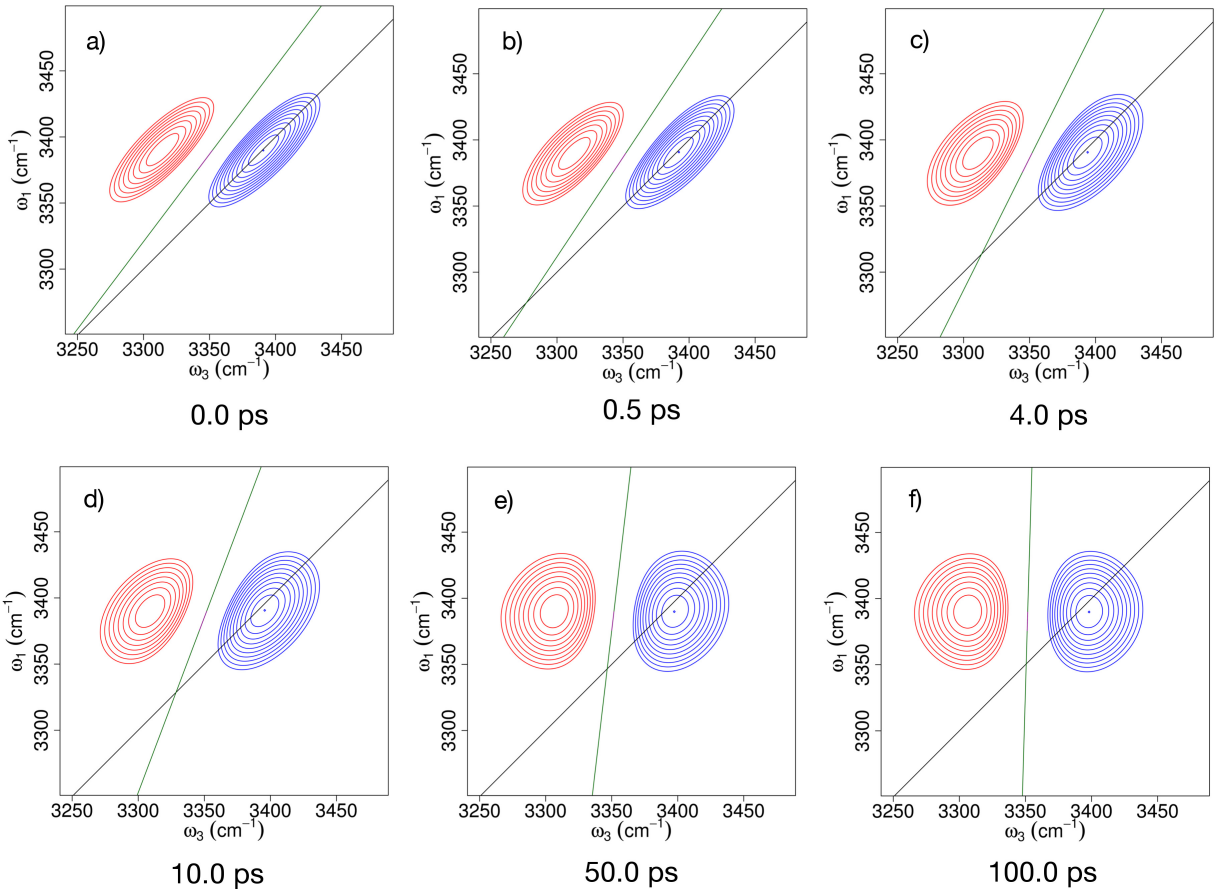

Figure 4: Simulated 2DIR spectrum for the MeOH -OH band for one molecule that remains within 2.5 Å of the surface for the entire 2.5 ns simulation. The delay times are: (a) $t_2 = 0.0$ ps, (b) $t_2 = 0.5$ ps, (c) $t_2 = 4.0$ ps, (d) $t_2 = 10.0$ ps, (e) $t_2 = 50.0$ ps and (f) $t_2 = 100.0$ ps.

while for MeOH in the bulk the dynamics is more rapid with $\tau_1 = 0.10$, $\tau_2 = 1.97$ and $\tau_3 = 18.15$ ps. This suggests that the dynamics at the surface is slowed-down by a factor of two to three. For the exchanging MeOH molecules the average FFCF also follows a multiexponential decay with time constants of $\tau_1 = 0.13$, $\tau_2 = 2.52$ and $\tau_3 = 27.42$ ps, i.e. bracketed by those of the surface-bound and bulk MeOH molecules. Due to sampling two different environments in the course of the dynamics, the fluctuation bars (indicating the minimum and maximum amplitude of the individual FFCFs) for those "exchanging" MeOH molecules increase after $\approx$ 15 ps, see Figure 5. Conversely, fluctuation bars of the surface-bound (red) and bulk-only (blue) MeOH molecules are considerably more narrow. The use of minimum/maximum values was preferred over more customary bootstrapping procedures because the analysis of MeOH molecules of each type does not lend itself to more comprehensive meaningful statistical analyses.

The dynamics can also be characterized by the time constants associated with the CLS, see inset Figure 5. Surface-bound and bulk MeOH were considered separately and only molecules which remained in the respective region (close to the surface or in bulk, respectively) for the entire 2.5 ns simulation time were analyzed. The time constants from fitting the data of the CLS for surface-bound (red symbols in Figure 5) MeOH are $\tau_1 = 0.09$ ps, $\tau_2 = 3.68$ ps and $\tau_3 = 42.05$ ps whereas for MeOH in the middle of the column (blue symbols) they are $\tau_1 = 0.04$ ps, $\tau_2 = 1.88$ ps and $\tau_3 = 17.94$ ps. As expected, these time scales are similar to those of the FFCF and confirm that the dynamics near the surface is considerably slowed-down.

To describe the structural properties of MeOH at the surface, the angular probability distribution function for the methanol-OH and methanol-OC vectors were analyzed, see Figure 6, left. For this, the angular probability distributions $P(\cos(\theta))$ are calculated for MeOH molecules within 2.5 Å of the silica surface oxygen atoms and compared with the distribution

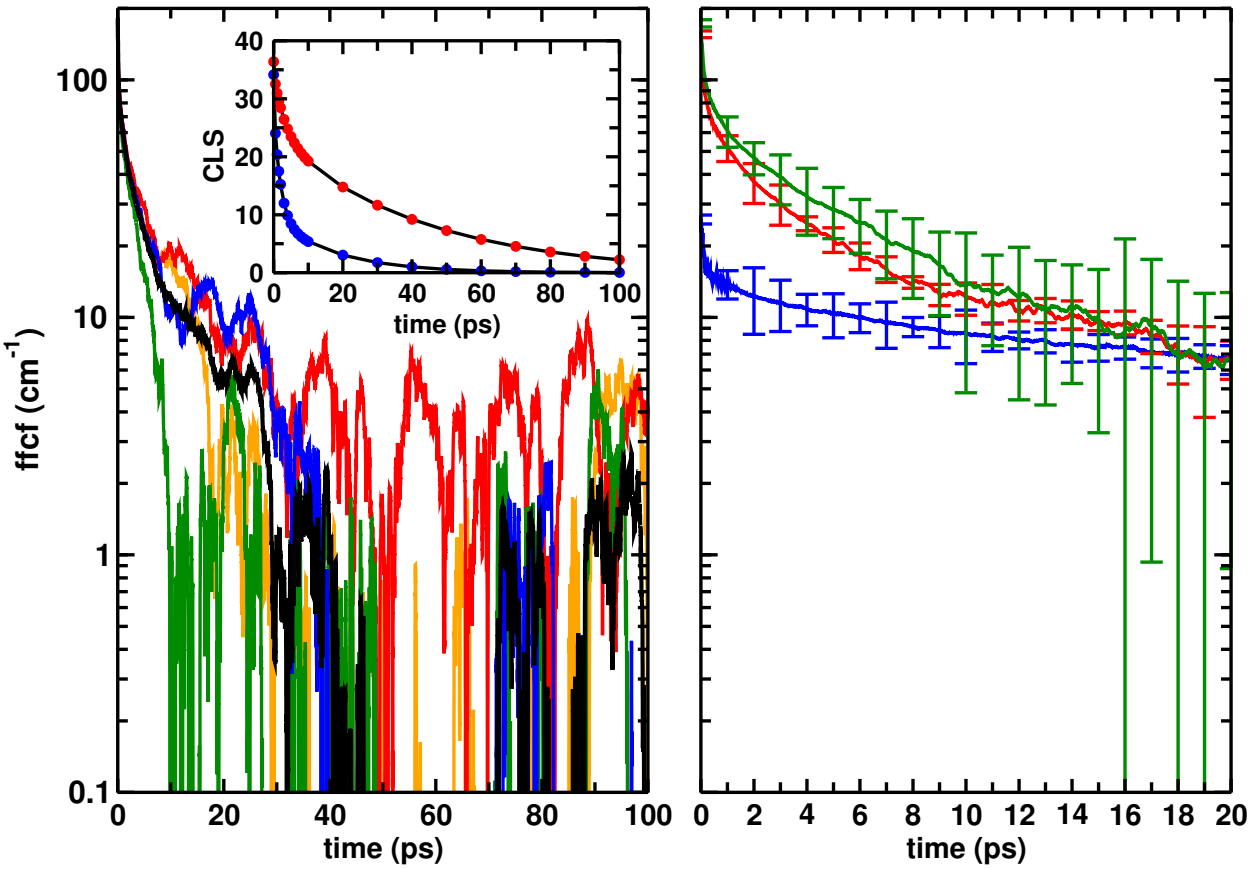

Figure 5: Left panel: The 4 individual FFCFs for surface-bound MeOH (color) and their average (black). Inset figure - Center line slope (CLS) as a function of delay time t_2 from the data in Figure 4. Right panel: The FFCFs averaged over 4 surface-bound (red) MeOH, 4 MeOH in the bulk (blue), and 4 MeOH which exchange (green) between surface and bulk as a function of lag time. The bars report the minimum and maximum value of the FFCF of the individual correlation functions. All $y-$axes are on a logarithmic scale.

functions for those further away than 2.5 Å.

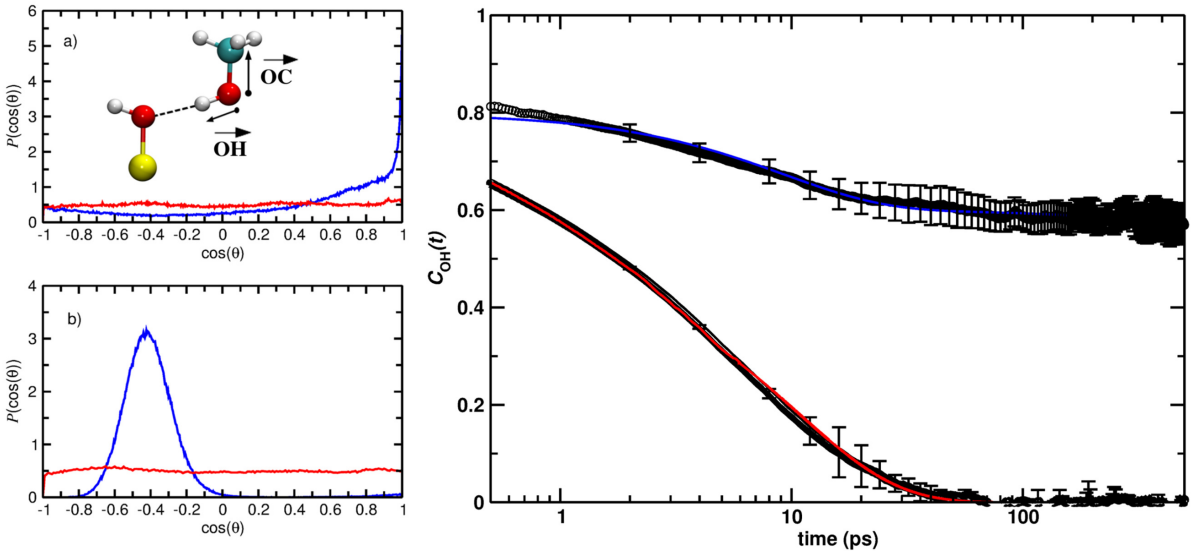

Figure 6: Left: Normalized probability distribution functions for the $-\overrightarrow{OC}$ (panel a) and $-\overrightarrow{OH}$ (panel b) vectors for MeOH molecules close to the surface (blue; $z < 2.5$ Å) and away from it (red; $z > 2.5$ Å). Right: Orientational auto-correlation function for the $-\overrightarrow{OH}$ unit vector for MeOH close to the surface ($z < 2.5$ Å, average over 10 MeOH) and away from the surface ($z > 2.5$ Å, average over 10 MeOH). Raw data in black and fit to stretched exponentials in red (MeOH in bulk) and blue (MeOH close to the surface), respectively. Fluctuation bars report the minimum and maximum value of the individual correlation functions. The $x-$ axis is logarithmic.

The averaging is carried out over all 10 MeOH molecules which remain within 2.5 Å of the silica surface during the entire simulation time. For MeOH closest to the silica layer ($z < 2.5$ Å), the $\overrightarrow{OC}$ orients perpendicular to the surface, as shown by the maximum probability for $cos(\theta) = 1$ ($\theta = 0°$) which is due to hydrogen bonding of the methanol-OH group to the surface -OH group, see Figure 6, left. Contrary to that, MeOH in the bulk solvent samples all directions.

Finally, the orientational dynamics of MeOH close to the surface and away from it can be characterized from considering reorientational autocorrelation functions. The analysis is

carried out for the $\overrightarrow{OH}$-unit vector $\hat{\rho}$

$$C_{\hat{\rho}}(t) = \frac{\langle \hat{\rho}(0)\hat{\rho}(t) \rangle}{\langle \hat{\rho}(0)\hat{\rho}(0) \rangle} \tag{8}$$

Figure 6, right, demonstrates that for MeOH close to the surface the orientational dynamics is considerably slower than in the bulk. The reorientational time scales are obtained from fitting to either a tri-exponential function $A_1 \exp(-t/\tau_1) + A_2 \exp(-t/\tau_2) + (1 - A_1 - A_2) \exp(-t/\tau_3)$, with decay constants τ_1 to τ_3, or to a stretched exponential $(e^{-t/\tau})^{\beta}$. For molecules close to the surface the relaxation times τ_1 to τ_3 are (0.2, 2.5, 535) ps whereas for those in the bulk they are (0.01, 1.0, 10) ps. Using a stretched exponential yields (τ = 3.4 ps, β = 0.5) for MeOH in the bulk and (τ = 21.0 ps, β = 0.2) for MeOH bound to the surface, respectively. These findings are consistent with the rotational relaxation of water at silica or other polar surfaces for which slower dynamics at the surface compared to that in bulk was found.[48–50] Such time decays have also been determined from MD simulations of water at the surface of hydrocarbons and reverse micelles.[51,52] The dipole reorientation correlation time for water at the surface of the hydrocarbon decays within $\approx$ 4 to 5 ps in simulations with the SPC/E water model and fitting to either single exponentials or a stretched exponential decay. In the latter case the $\beta-$ parameter ranges from 0.17 to 0.37 for water inside the reverse micelle and the orientational correlation function was found to remain significantly above 1 % of its initial value by 1 ns.[52] In the present case, the amplitude by 0.5 ns was still 40 % which is probably due to the strong interaction and alignment of the MeOH-OH bond towards the surface -OH group.

The present study suggests that the dynamics of MeOH at the solid/liquid interface between a silica support and the mixed solvent is slowed down by at least a factor of two compared to the dynamics in the mixed solvent. This is concluded from the decorrelation times of the frequency-frequency correlation function. Such a difference should be observable with

surface-sensitive spectroscopic techniques such as 2-dimensional sum frequency generation spectroscopy (2D-SFG) which is related to two-dimensional IR (2D-IR) spectroscopy. Both techniques can probe structural dynamics in condensed phase systems on the picosecond time scale.[45] Furthermore, recent computational work has established that 2D-IR and 2D-SFG spectroscopies probe similar dynamics.[53] Therefore, the information contained in the FFCF discussed here should provide a starting point for surface-sensitive characterization of idealized and more realistic chromatographic systems.

Structural characterization of the silica//MeOH/water interface is of considerable practical interest, particularly for applications in chromatography. These systems have found to be more highly hydrated than typically suspected and the solvent is likely to play an active role in adsorption/desorption and hence influence elution times and retention. It is expected that including the alkyl chains increases the heterogeneity and probably further slows down the dynamics of surface-bound solvent molecules. It is proposed to use optical - in particular 2D-SFG - spectroscopy to characterize the chemical environment of heterogeneous interfaces relevant to high performance and reversed phase liquid chromatography. The spectroscopic signatures should be sufficiently distinct from the bulk signal to allow this. Such information will be very valuable to move towards rational design of chromatography environments based on physico-chemical data.

Compared to previous work, the present study confirms the pronounced heterogeneous dynamics at the solid/liquid interface involving hydroxylated silica.[9,13,14] Previous simulations have already suggested that nonexponential dynamics is expected for solvent molecules close to the stationary phase and the present simulations provide another example for this observation. Quantitatively, the present work points towards a slowdown of the dynamics by a factor of two. This is consistent with the jump model[54,55] which has been used to interpret the reorientational dynamics of water close to other solutes, including chloride ions,[56]

cyanide,[36] or -OH groups in hydrophilic environments.[14]

Conclusions

The present work reports all-atom molecular dynamics simulations of the structure and dynamics of a water/MeOH mixture and vibrational spectroscopy of MeOH at hydroxylated silica surfaces. The key information obtained from the computed 2D-IR spectrum is the central line slope (CLS), which can be directly compared with surface-sensitive spectroscopic experiments. The time constants associated with the CLS and the FFCF characterize the relaxation time for different dynamical processes. From the present study, it is found that orientational dynamics for surface bound MeOH is slowed down approximately by a factor of 2 compared to MeOH in the bulk. These observables can be obtained experimentally and provide quantitative atomistic detail of solvent mixtures at interfaces relevant to chromatography.

Acknowledgement

Support by the Swiss National Science Foundation through grants 200021-117810, the NCCR MUST (to MM), and the University of Basel is gratefully acknowledged.

References

(1) Rafferty, J. L.; Siepmann, J. I.; Schure, M. R. *J.Chromatogr. A* **2008**, *1204*, 11–19.

(2) Rafferty, J. L.; Siepmann, J. I.; Schure, M. R. *J.Chromatogr. A* **2012**, *1223*, 24–34.

(3) Braun, A., J. Fouqueau; Meuwly, M.; Bemish, R. J. *Phys. Chem. Chem. Phys.* **2008**, *10*, 4765–4777.

(4) Gupta, P. K.; Meuwly, M. *J. Phys. Chem. B* **2012**, *116*, 10951–10959.

(5) Margelefsky, E. L.; Zeidan, R. K.; Davis, M. E. *Chem. Soc. Rev.* **2008**, *37*, 1118–1126.

(6) Brunelli, N. A.; Venkatasubbaiah, K.; Jones, C. W. *Chemistry of Materials* **2012**, *24*, 2433–2442.

(7) Du, Q.; Superfine, R.; Freysz, E.; Shen, Y. R. *Phys. Rev. Lett.* **1993**, *70*, 2313–2316.

(8) Roy, D.; Liu, S.; Woods, B. L.; Siler, A. R.; Fourkas, J. T.; Weeks, J. D.; Walker, R. A. *J. Phys. Chem. C* **2013**, *117*, 27052–27061.

(9) Hu, Z.; Weeks, J. D. *J. Phys. Chem. C* **2010**, *114*, 10202–10211.

(10) Heinz, T. F.; Tom, H. W. K.; Shen, Y. R. *Phys. Rev. A* **1983**, *28*, 1883–1885.

(11) Scott, R. P. W. *Faraday Symp. Chem. Soc.* **1980**, *15*, 49–68.

(12) Karnes, J. J.; Gobrogge, E. A.; Walker, R. A.; Benjamin, I. *J. Phys. Chem. B* **2016**, *120*, 1569–1578.

(13) Gupta, P. K.; Meuwly, M. *Farad. Discuss.* **2013**, *167*, 329–346.

(14) Laage, D.; Thompson, W. H. *J. Chem. Phys.* **2012**, *136*, 084509.

(15) Giovambattista, N.; Debenedetti, P. G.; Rossky, P. J. *Proc. Nat. Acad. Sci. USA* **2009**, *106*, 15181–15185.

(16) Lee, S.; Rossky, P. *J. Chem. Phys.* **1994**, *100*, 3334–3345.

(17) Orzechowski, M.; Meuwly, M. *J. Phys. Chem. B* **2010**, *114*, 12203–12212.

(18) Fountain, K. J.; Xu, J.; Diehl, D. M.; Morrison, D. *J. Sep. Sci.* **2010**, *33*, 740–751.

(19) Reimers, J. R.; Hall, L. E. *J. Am. Chem. Soc.* **1999**, *121*, 3730–3744.

(20) Braun, J.; Fouqueau, A.; Bemish, R. J.; Meuwly, M. *Phys. Chem. Chem. Phys.* **2008**, *10*, 4765–4777.

(21) Jorgensen, W. L.; Chandrasekhar, J.; Madura, J. D.; Impey, R. W.; Klein, C. L. *J. Chem. Phys.* **1983**, *79*, 926–935.

(22) Vanommeslaeghe, K.; Hatcher, E.; Acharya, C.; Kundu, S.; Zhong, S.; Shim, J.; Darian, E.; Guvench, O.; Lopes, P.; Vorobyov, I.; Jr., A. D. M. *J. Comput. Chem.* **2010**, *31*, 671–690.

(23) Bauschlicher, C. W.; Langhoff, S. R.; Walch, S. P. *J. Chem. Phys.* **1992**, *96*, 450–454.

(24) Chu, P.; Guenther, F.; Rhoderick, G.; Lafferty, W. *J. Res. Natl. Inst. Stand. Technol.* **1999**, *104*, 59–81.

(25) Brooks, B. R.; Bruccoleri, R. E.; Olafson, B. D.; States, D. J.; Swaminathan, S.; Karplus, M. *J. Comput. Chem.* **1983**, *4*, 187–217.

(26) Ryckaert, J. P.; Ciccotti, G.; Berendsen, H. J. *J. Comput. Phys.* **1977**, *23*, 327–341.

(27) Cazade, P.-A.; Bereau, T.; Meuwly, M. *J. Phys. Chem. B* **2014**, *118*, 8135–8147.

(28) Yamaguchi, T.; Hidaka, K.; Soper, A. K. *Mol. Phys.* **1999**, *96*, 1159–1168.

(29) Haughney, M.; Ferrario, M.; McDonald, I. R. *J. Phys. Chem.* **1987**, *91*, 4934–4940.

(30) Patel, S.; Brooks, C. L. *J. Chem. Phys.* **2005**, *122*, 024508–10.

(31) Handgraaf, J.-W.; van Erp, T. S.; Meijer, E. J. *Chem. Phys. Lett.* **2003**, *367*, 617 – 624.

(32) Soper, A. *Chem. Phys.* **2000**, *258*, 121–137.

(33) Herzberg, G. *Molecular spectra and molecular structure. Vol.2: Infrared and Raman spectra of polyatomic molecules, New York: Van Nostrand, Reinhold*; 1945.

(34) Falk, M.; Whalley, E. *J. Chem. Phys.* **1961**, *34*, 1554–1568.

(35) Laenen, R.; Gale, G.; Lascoux, N. *J. Phys. Chem. A* **1999**, *103*, 10708–10712.

(36) Lee, M. W.; Carr, J. K.; Göllner, M.; Hamm, P.; Meuwly, M. *J. Chem. Phys.* **2013**, *139*, 054506.

(37) Plattner, N.; Meuwly, M. *J. Mol. Model.* **2009**, *15*, 687–94.

(38) Lin, B.; Lopes, P. E. M.; Roux, B.; MacKerell, A. D., Jr. *J. Chem. Phys.* **2013**, *139*, 084509.

(39) Torii, H. *J. Phys. Chem. A* **1999**, *103*, 2843–2850.

(40) Zheng, R.; Sun, Y.; Shi, Q. *Phys. Chem. Chem. Phys.* **2011**, *13*, 2027–2035.

(41) Ghosh, M. K.; Lee, J.; Choi, C. H.; Cho, M. *J. Phys. Chem. A* **2012**, *116*, 8965–8971.

(42) Sieffert, N.; Buehl, M.; Gaigeot, M.-P.; Morrison, C. A. *J. Chem. Theo. Comput.* **2013**, *9*, 106–118.

(43) Sieffert, N.; Buehl, M.; Gaigeot, M.-P.; Morrison, C. A. *J. Chem. Theo. Comput.* **2013**, *9*, 106–118.

(44) Bertie, J.; Zhang, S. *J. Mol. Struct.* **1997**, *413*, 333–363.

(45) Hamm, P.; Zanni, M. *Concepts and Methods of 2D Infrared Spectroscopy*; Cambridge University Press, 2011.

(46) Schmidt, J.; Roberts, S.; Loparo, J.; Tokmakoff, A.; Fayer, M.; Skinner, J. *Chem. Phys.* **2007**, *341*, 143 – 157.

(47) Péron, J.; Sandorfy, C. *J. Chem. Phys.* **1976**, *65*, 3153–3157.

(48) Argyris, D.; Cole, D. R.; Striolo, A. *J. Phys. Chem. C* **2009**, *113*, 19591–19600.

(49) Argyris, D.; Ho, T.; Cole, D. R.; Striolo, A. *J. Phys. Chem. C* **2011**, *115*, 2038–2046.

(50) Tan, O. Z.; Tsai, K. H.; Wu, M. C. H.; Kuo, J.-L. *J. Phys. Chem. C* **2011**, *115*, 22444–22450.

(51) Chowdhary, J.; Ladanyi, B. M. *J. Phys. Chem. B* **2009**, *113*, 4045–4053.

(52) Pieniazek, P. A.; Lin, Y.-S.; Chowdhary, J.; Ladanyi, B. M.; Skinner, J. L. *J. Phys. Chem. B* **2009**, *113*, 15017–15028.

(53) Roy, S.; Gruenbaum, S.; Skinner, J. *J. Chem. Phys.* **2014**, *141*, 22D505–9.

(54) Ivanov, E. N. *Sov. Phys., JETP* **1964**, *18*, 1041–1045.

(55) Laage, D.; Stirnemann, G.; Sterpone, F.; Rey, R.; Hynes, J. T. *Annu. Rev. Phys. Chem.* **2011**, *62*, 395–416.

(56) Laage, D.; Hynes, J. T. *Proc. Nat. Acad. Sci. USA* **2007**, *104*, 11167–11172.